Development of an efficient solar concentrator and utilization in copper extraction from copper minerals

K. Yang [a], Y. Nahmad-Molinari [b]*, L.F. Camacho-González [b], F.M. de los Santos-García [b], A. Lopéz-Valdivieso [a]*

[a]Universidad Autónoma de San Luis Potosí, Instituto de Metalurgia.San Luis Potosí, Mexico.
[b]Universidad Autónoma de San Luis Potosí, Instituto de Fisica. San Luis Potosí, Mexico.
E-mail: Ke Yang: A293258@alumnos.uaslp.mx. Luis Fernando Camacho González: fernandocamacho-glz@gmail.com. Fátima MI de los Santos García: fatima.desantosgarcia@uaslp.mx.
Yuri Nahmad Molinari*: yuri@ifisica.uaslp.mx. Alejandro Lopéz Valdivieso*: alopez@uaslp.mx.

(Received 22 February 2024; Accepted 16 December 2024)

Abstract

A novel and cost-effective solar concentrator has been developed to enhance efficient copper extraction. Based on the criteria for a stationary compound parabolic concentrator, the reflector geometry incorporates a half-spherical curve and a strength line. This design significantly improves the concentrator's ability to capture more marginal rays compared to widely used commercial solar concentrators. In this study, a newly configured solar concentrator was constructed with aluminum sheet and tested in San Luis Potosi, Mexico, with a comprehensive performance analysis. The investigation revealed an optical efficiency of 0.73 and a maximum thermal efficiency of 68%. Experimental results demonstrated that the solar collector could absorb solar radiation throughout the year without the need for a tracking system. It efficiently facilitated the copper sulfide ore leaching process at a medium temperature of approximately 70 °C. Capital cost analysis indicated an exceptionally low unit manufacturing cost of only $125 USD /$m^2$. The study further proposes that the implementation of this solar collector could potentially double the copper recovery rate and triple the annual increase in copper cement without contributing to CO_2 emissions. Additionally, the feasibility of deploying this new concentrator on an industrial scale was thoroughly evaluated to provide a substantial support for advancing cleaner copper production technology through further innovation.

Keywords: solar energy; net-zero carbon emissions; compound parabolic collectors; acid leaching; copper recovery

Abbreviations

CPC, compound parabolic concentrator; **LX,** agitation leaching; **SX**, solvent extraction; **EW**, electrowinning.; **STC**, solar thermal collector; **PTC**, parabolic trough concentrator

1. Introduction

Excessive CO_2 emissions represent a critical global environmental challenge, necessitating a 45% reduction by 2030 and achieving net-zero emissions by 2050, as outlined in the Paris Agreement [1]. In 2020, a significant movement for Net-Zero carbon emissions emerged, urging governments to demonstrate genuine commitment to carbon neutrality. Subsequent studies proposed essential engineering frameworks for reducing rare-metal costs and mitigating harmful environmental impacts in natural gas hydration and drilling[2-4]. Addressing this, the reduction of CO_2 emissions from the industry sector is imperative, given its contribution of 25% to global annual emissions and 37% of fossil fuel consumption worldwide in 2022[5]. Solar technology has emerged as a promising alternative to fossil fuels, with substantial developments aimed at reducing CO_2 emissions.

Integrating solar technologies into energy-intensive industries' production processes is appealing. Recent investigations into stationary compound parabolic concentrators (CPC) have evaluated their performance, efficiency, and costs, demonstrating the efficiency achievable with these concentrators while concurrently reduction in costs[6, 7]. Similarly, Ahmadi et al. designed a solar concentrator with a flat bottom and parabolic-curved sides, achieving an optical efficiency of 0.8 at a manufacturing cost of $250 [8]. Martin explored the use of 3D-printing technology to reduce CPC costs to $490, significantly lower than those of commercial counterparts [9]. Most concentrators, as observed in previous research, adopt parabolic profiles for their reflector geometry, which often require precise manufacturing processes and result in higher costs.

Copper, a major industrial metal, is experiencing continuous growth in demand. Low-grade copper sulfide ores, including chalcocite (Cu_2S) and covellite (CuS), account for 90% of total copper production. Hydrometallurgy, which constitutes 20% of primary copper production, involves flotation to produce a copper concentrate[10, 11]. This concentrate is then processed at high temperatures to extract copper from the mineral. An alternative process , leaching, offers advantages over pyrometallurgical techniques by avoiding SO_2 gas emissions and enabling the direct conversion of dissolved copper into metallic copper[12]. However, copper sulfides exhibit slow leaching kinetics at 25°C, necessitating high-temperature leaching to improve the process [13, 14]. Despite the benefits of solar thermal collectors (STC) in reducing energy consumption and CO_2 emissions during leaching processes, their adoption is hindered by high investment costs. The capital cost of STC with a thermal storage system range from USD5000/kW to USD10500/kW, compared to USD3000-8400/kW for coal plants[15]. consequently, the attractiveness of solar collectors is diminished by the substantial increase in capital costs. This study aims to design an economical, efficient, and easily manufacturable STC to enhance copper recovery in extraction processes. The focus is on utilizing solar energy for leaching secondary copper sulfides by employing a novel solar concentrator design to convert solar radiation into heat for the agitation copper leaching process.

2. Design of a new solar thermal concentrator

Solar concentrators are categorized into imaging and non-imaging forming systems, depending on whether sun rays are focused within a point, a focus line, or neither. The parabolic trough concentrator (PTC), concentrating solar rays to its focus, is widely acknowledged as the most mature and commercialized thermal technology, extensively employed in high-temperature industrial processes. However, its reflector geometry limits acceptance to solar rays within a specific narrow angle, necessitating a tracking system to enhance efficiency, thereby incurring additional capital costs. Another trough-type technology, the Compound Parabolic Concentrator (CPC), utilizes a reflector formed by combining two symmetric parabolic segments with different focal lengths. This geometric profile efficiently concentrates solar rays to a wide aperture within an acceptance angle, allowing CPCs to operate without a continuous tracking system and achieving higher thermal efficiency. Studies indicate that it can attain temperatures between 60-150°C for most industrial processes with medium-temperature requirements, making CPC suitable for the expected operating range of 50-80°C in leaching processes [16].

Traditional CPC always adopts the parabolic reflector geometry and cartesian ovoid, considered theoretically perfect focalizing surfaces for creating lenses. However, these geometries present challenges in manufacturing processes and result in high costs. In 2016, the successful application of the Five-hundred-meter Aperture Spherical radio Telescope (FAST) demonstrated that a spherical surface used as a focalizing surface could substitute the parabolic shape at lower costs[17]. Fig.1 Illustrates the concentrator's geometry, presenting its configurations during both the summer solstice and the winter solstice.

2.1 Material and method

This work adopts a half-spherical curve as the reflector geometry, drawing inspiration from the spherical surface of FAST. To illustrate the reflection of rays in the concentrator, representative cases are selected for solar incident rays at noon during the summer and winter solstices. In Fig.1(a), when the sun is directly overhead at noon above the Tropic of Cancer on the summer solstice, Sector ADE represents the paraxial zone, reflecting all incident rays within this sector to Point C, forming a caustic line. Fig.1(b) illustrates solar rays

concentrating most directly on the Tropic of Capricorn at noon during the winter solstice. The paraxial zone shifts from Sector ADE to Sector AD'E', reflecting incident rays within this sector to Point C'. Fig. 2 demonstrates that Sector AD'E is an overlap area of Sector ADE and AD'E' as the sun moves from the Tropic of Cancer to the Tropic of Capricorn. This overlap indicates that all incident rays within Sector AD'E are reflected to the vicinity of points C and C'. Consequently, the heat receiver can be positioned from Point C to Point C' to receive solar rays consistently from spring to winter without positional changes.

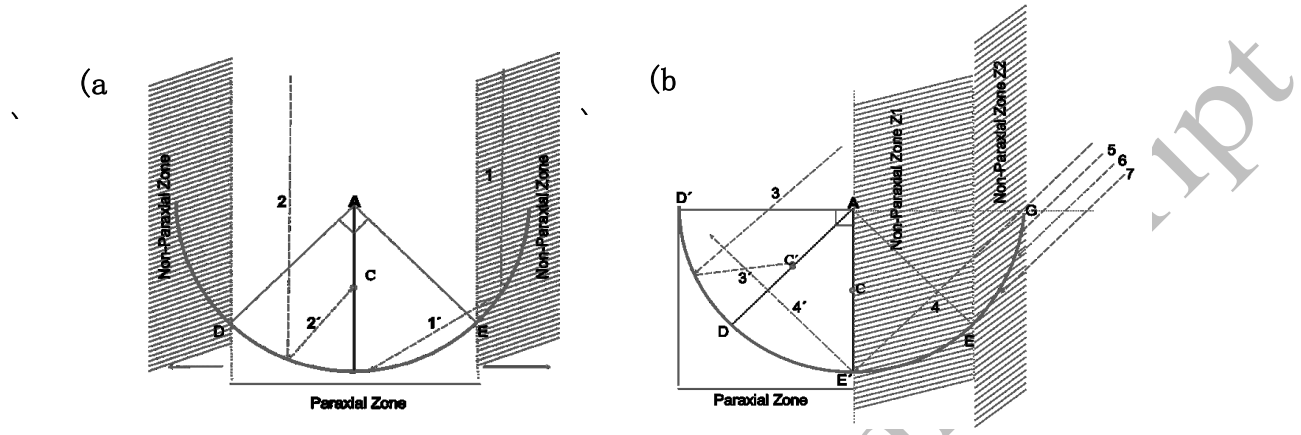

Figure 1. Geometry of the concentrator: (a) on summer solstice and (b) on winter solstice.

The arc EG on the right-hand side of the half-spherical curve in Fig.2 is replaced with a straight in EF. This modification offers two advantages: The line EF is easier and more cost-effective to manufacture compared to the arc EG; 2) While the arc EG in Fig. 2(a) tends to shed a significant amount of incident rays, the line EF in Fig. 2(b) has the advantage of capturing the most marginal ray.

The angle (θ) formed between the line EF and the horizon is twice the latitude angle of 22.1°. This implies that during spring and winter, when the sun's path is within this wedge, a substantial portion of direct solar radiation can be efficiently collected.

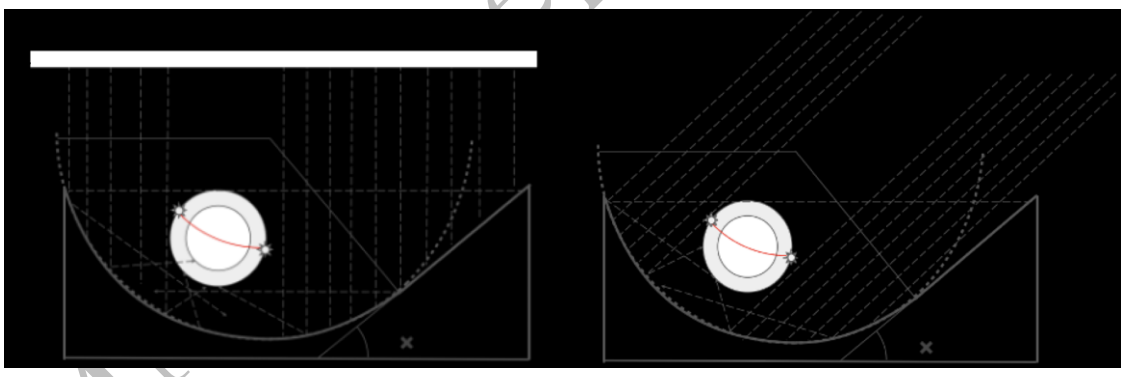

Figure 2. Illustration of ray tracing for the concentrator: (a) on summer solstice and (b) on winter solstice.

In accordance with the function involving the acceptance angle (θ_c) and geometrical concentration ratio (C_{geom}), the calculated C_{geom} should be 1.43x [18]. The acceptance angle of this concentrator (θ_c) measures 44.2°, equivalent to twice the latitude angle. Other geometric sizes are listed in Table 1.

Table 1. Geometry of the new concentrator.

Parameters	Dimension(m)
Width of the collector	0.22

Length of the collector	1.80
Height of the collector	0.10
Curvature radius of the half-spherical curve	0.10

In addition to the acceptance angle ±θc, the optical performance is further characterized by optical efficiency. In practical applications, the value can be roughly estimated from the performance parameters of the materials used in the collector. The optical efficiency is calculated using the formula[18]:

$\eta_{optical}=\tau_1 \tau_2^{\wedge(n)} \alpha (1-L) \Gamma$ (1)

where τ_1 and τ_2 are the transmittance of the outer envelope of the heat receiver and the reflectivity of the concentrator surface respectively, (n) is the average number of reflections, α is the absorptance of the coating surface, L is any geometric loss due to the gap between the heat receiver and the concentrator, and Γ is the fraction of the incident solar radiation accepted by the concentrator after correction for ¨loss of diffuse¨. The optical losses include geometric, reflection and absorption losses.

All parameters are listed in Table 2. The τ_1, τ_2, α and (n) are provided by the material suppliers. Γ is characterized by the geometrical concentration ratio C_{geom}. An ideal low-concentration collector should be able to gather about 1/ C_{geom} of the diffuse insolation [18].If a typical diffuse fraction is assumed to be 12%, Γ is estimated as follows:

$\Gamma=88\%+12\%*1/ C_{geom}$ (2)

Where the direct isolation fraction is 88%, Γ is estimated as 0.97 at $C_{geom} \cong 1.43\times$

The geometric loss L is given by:

$L \cong g/\pi r$ (3)

Where g represents a gap between the reflector and the absorber surface and r is an absorber radius. As a result, the optical efficiency $\eta_{optical}$ of our newly designed concentrator is 0.73.

Table 2. Performance Parameters for concentrator.

Parameter	symbol	Value
Transmittance of outer envelope of the heat receiver (polycarbonate)	τ1	0.9
The reflectivity of the concentrator surface (Alumina)	τ2	0.95
Average number of reflections	(n)	0.8
Absorptance of coating surface	α	0.95
Gap loss	L	0.076 (Eq.3)
Correction for loss of diffuse	Γ	0.97
Optical efficiency	$\eta_{optical}$	0.73 (Eq.1)

A numerical simulation was conducted using COMSOL Multiphysics to investigate the concentration performance of the new concentrator throughout the year without any tracking system. The 15th day of each month, excluding February, July, September, and December was randomly selected as the focus of the simulation. The solar flux distribution on the surface of the heat receiver predominantly relies on the daily solar irradiation, geometric properties of the concentrator, and thermophysical properties of the heat receiver.

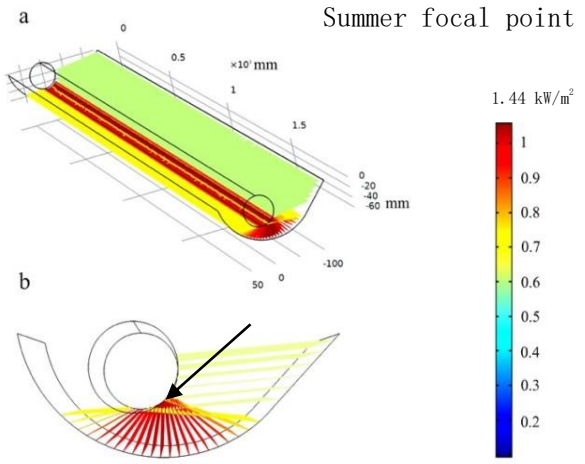

Figure 3. (a) Solar flux distribution on the absorber surface and (b) cross-section on summer solstice (20/7/2023).

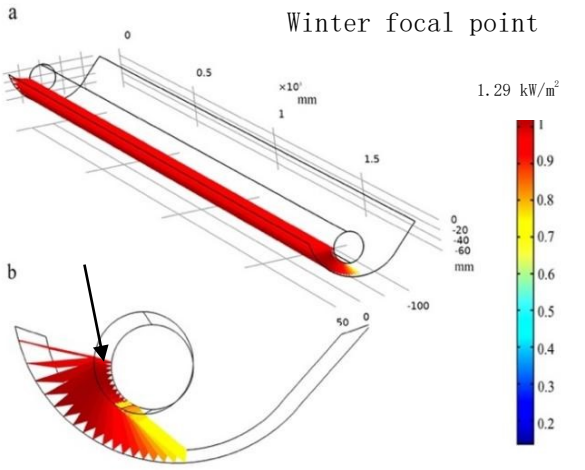

Figure 4. (a) Solar flux distribution on the absorber surface and (b) cross-section on winter solstice (21/12/2023).

COMSOL has the capability to automatically adjust the sun's geographic location based on a specified day or hour. Assuming a solar peak irradiation of 1kW/m^2, 10^5 solar rays are randomly directed towards the tube at various times during different seasons. The distributions of solar flux on the tube's surface during summer and winter solstice are obtained and illustrated in Fig.3 and Fig.4. In Fig.3, the maximum energy flow reaches 1.44 kW/m^2 at the summer focal point, representing a 44% increase in energy input. Calculably, the tube receives few rays, and the focal point shifts from the right side to the left as the solar incident angle decreases throughout the day of the winter solstice. Consequently, the maximum energy flow at the winter focal point is 1.29 kW/m^2, with the collector enhancing the energy input by 29%.

The new concentrators are fabricated using aluminum sheets (0.3mm thickness, 40 Brinell hardness), as depicted in Fig.5. Aluminum foundations support them, utilizing the same material as concentrators. The aluminum foundations are filled with polyurethane foam to minimize heat losses between the concentrator and the floor.

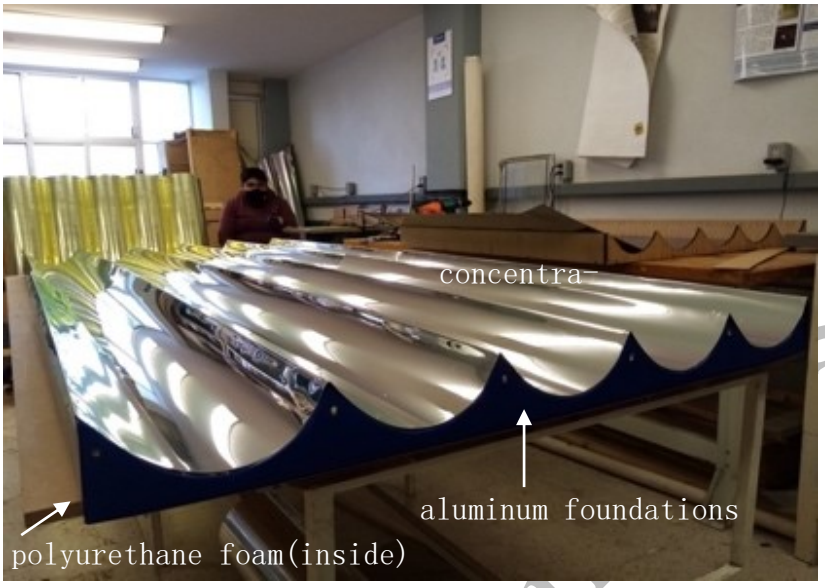

Figure 5. The new concentrator.

2.2. Laboratory setup

Copper minerals with a total copper grade of 1.45%, including 53.79% secondary copper sulfide were sourced from a mine in Mexico. The particle size ranged from 40-250um. The lixiviant, holding 3L water, 0.23 kg ferric sulfate (19.5w Fe^{3+}), and 26 ml acid sulfate (95%-98%w), was heated to 50°C, 60°C, and 70°C, respectively. A 1.16 kg sample was added in suspension in the lixiviant and stirred for 2h (the solid-to-liquid ratio of the slurry is 0.4). The initial concentration of Fe^{3+} and H^{+} in the aqueous solution was 15g/L. Ten milliliters of slurry was extracted each time at 3min, 5min, 10min, 20min, 30min, 45min, 60min, 90min, and 120min. The liquid samples were filtered and diluted for assay. All solid samples were filtered, cleaned, dried, and prepared for Cu^{2+} assay.

Blackened aluminum tubes were utilized as receivers instead of glass evacuated tubes to prevent breakage during installation, as illustrated in Fig.6. To ensure optical accuracy, the black tubes are fixed in the vicinity of points C and C' by plastic plates, as shown in Fig.2. The collectors were sealed with polycarbonate covers, and the air trapped between the tube and cover formed a greenhouse effect, reducing conductive and convective heat losses. The water tank volume expanded to 1000L with a 25m^2 solar collector area. All PVC pipes used in the system were wrapped with polyurethane.

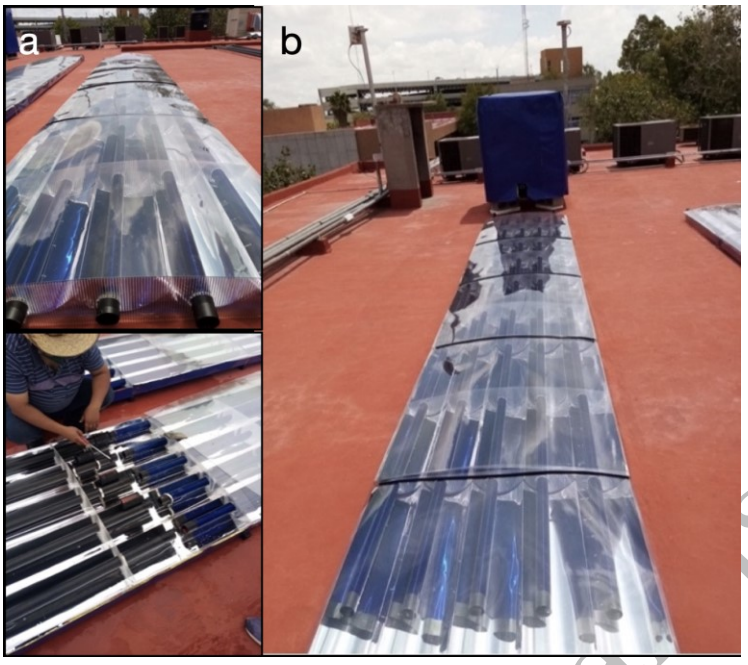

Figure 6. New solar collector (a) Overall and internal structure of collector; (b) Water tank and collector.

2.3. Optical and thermal experiments

The test was conducted on the roof of a building in Universidad Autónoma de San Luis Potosí, Mexico. The experiments were conducted from 9:00 to 18:00, and cold water was drained from the tank and circulated through the collector. An ambient temperature sensor was placed in a shelter above the ground and shielded from direct insolation. All temperature data from the thermometers were acquired every 10 seconds. A pyranometer (CM22, Kipp&Zonen, ±5%) and a pyrheliometer (CHIP, Kipp&Zonen, ±5%) were placed on the aperture area of the CPC to measure the global solar irradiation (G_g) and the direct normal irradiation (G_{DN}), respectively. The solar irradiation that entered the concentrator's aperture area (Gcpc) was calculated through Eq.4-7[19]:

$$Gcpc=G_{dp}+G_d \quad (4)$$

$$Gdp=G_{DN}\times\cos(\theta) \quad (5)$$

$$Gd=(Gg-Gdp)/Cgeom \ (\text{if } (\beta+\theta_A)<90^\circ) \quad (6)$$

where G_{dp} and G_d are the direct and the diffuse solar irradiations entering the CPC trough aperture area, W/m^2, G_g global solar irradiation and G_{DN} the direct normal irradiation. geometrical concentration ratio, θ_A is the incidence angle, β is the tilt angle of the CPC, 23.5º. Correspondently, the incidence angle θ is estimated by the following expression (for a south facing, tilted surface in the Northern Hemisphere):

$$\cos(\theta)=\sin(La-\beta)\sin\delta+\cos(L-\beta)\cos(\delta)\cos(h) \quad (7)$$

where, La is the latitude, 23.5º, δ is the solar declination, and h is the hour angle (negative-east, positive-west). The incident angle is retrieved from the National Renewable Energy Laboratory Solar Position Algorithm platform (SPA)[20].

Considering that the sun moves along a path within the acceptance angle of the concentrator throughout the day on equinox days due to the transversal projection of the incidence angle on that day, it is inferred that the concentration performance during equinox days is better than that on solstice days. Given that the solar irradiation in March is the highest, the spring equinox day is selected to investigate optical and thermal performances.

3. Performance tests of the new solar concentrator

3.1. Optical performance

The measured values for global solar irradiation (G_g), direct normal irradiation (Gcpc), and solar irradiation entering the concentrator's aperture area (Gcpc) are presented in Fig. 7. G_g fluctuates between 400-1000 W/m^2, while G_{DN} ranges between 300-600 W/m^2. Consequently, the solar irradiation entering the concentrator's aperture area (Gcpc), calculated using Eqs. 4-6, falls within the range of 200-700 W/m^2. This indicates that approximately 50%-70% of G_g is effectively collected. The Gcpc curve remains higher than the G_{DN} curve between 9:00 and 16:00, showcasing the concentrator's ability to gather about 1/ C_{geom} of the diffuse insolation. However, after 16:00, the Gcpc curve descends below the G_{DN} curve, indicating the cessation of direct solar radiation collection as the sun moves outside the acceptance angle.

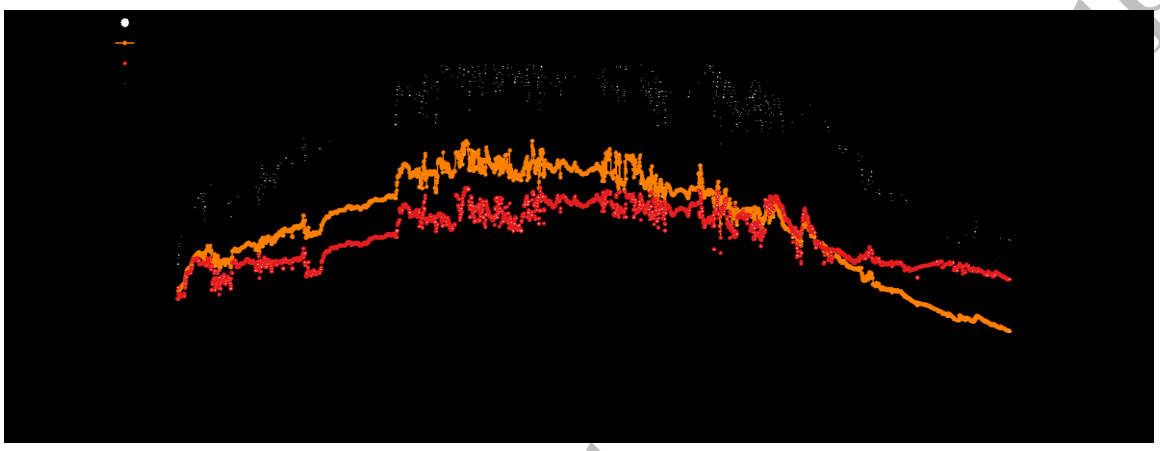

Figure 7. Solar irradiation within a daily test in San Luis Potosi, Mexico on March 20, 2023.

3.2. Thermal performance

The thermal experiments commenced from 8:00 on March 20 and extended until 18:00 on March 23, spanning a continuous duration of 32 h. The pump was activated at 8:00 and deactivated at 15:00. Subsequently, the pump was restarted, and water reheating occurred at 10:30 the following day. A thermometer (PT 1000) with a measuring error of ±0.1^{o}K was strategically placed in the tank to monitor water temperature. Data logging occurred every 10 seconds to record the water temperature.

The water temperature gradually increased from 25 ^{o}C to 83^{o}C at 14:00, followed by a gradual decrease at 15:00, indicating that the heat output surpassed input during this period. Consequently, the temperature naturally decreased from 80^{o}C to 70^{o}C at 10:30 the next day. Subsequently, the temperature began to rise again when the pump was restarted, reaching a maximum of 92^{o}C at 14:30. This observation indicates superior thermal efficiency and insulation of the testing system when the pump was turned off.

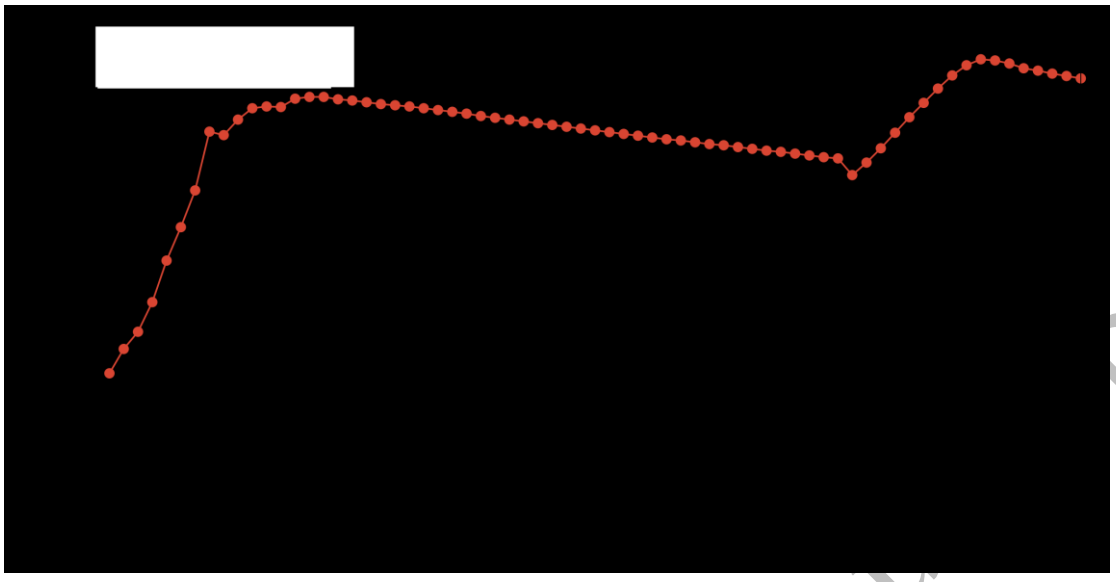

Figure 8. Water temperature change as a function of solar time in San Luis Potosi, Mexico.

The instantaneous thermal efficiency of the solar collector was calculated using Eq.8 below:

$$\eta_{themal}=(T_{water}-T_{ambient})/G_g \quad (8)$$

Where T_{water} is the water temperature in the storage tank and $T_{ambient}$ is the ambient temperature. According to the measured results in Fig.8, it can be found that the maximum thermal efficiency η_{themal} is 68% and the average value is 42%.

4. Copper sulfide ore leaching

4.1 Material and method

Minera Rio Tinto, a small copper mine in Chihuahua, Mexico, possesses copper ores with a total grade of 1.45% Cu and an acid-soluble copper grade of 1.42%. Following the current milling circuit, the particle size varies from 40-250μm. The elemental chemical assay of the ore is presented in Table 3. It indicates that copper exists in different forms: 21.38% as copper sulfate ($CuSO_4$), 22.76% as copper oxide (CuO and Cu_2O copper mineral species), 53.79% as secondary copper sulfide (Cu_2S and CuS), and 2.07% as primary copper sulfide ($CuFeS_2$ and Cu_5FeS_4).

Table.3 Chemical composition of the copper sulfide ore sample

	Mineral					Total
	Copper soluble in water	Copper soluble in acetic acid	Copper oxide	Secondary copper sulfide	Primary Copper sulfide	
Ore assay %	0.026	0.284	0.330	0.780	0.030	1.45
Distribution %	1.79	19.59	22.76	53.79	2.07	100

A Scanning Electron Microscope (SEM-EDS, JSM-6610LV, JEOL) was employed for the analysis of mineral species in the ore and copper species remaining in the residue. The chemical analysis of samples was conducted using an Atomic Absorption Spectrophotometer (AAS), specifically a Perkin Elmer 3110.

The results of the ore before leaching are depicted in Fig. 9. The analysis revealed the presence of Cu_2S in various forms within the ore, including coating on pyrite particles (FeS_2), within cracks of pyrite particles, coated by iron hydroxide ($HFeO_2$), kyanite (Al_2SiO_5), and other mineral structures. Additionally, Bornite

(Cu_5FeS_4), chalcopyrite ($CuFeS_2$), and copper sulfate ($CuSO_4$) were identified in the sample, along with some non-stoichiometric sulfate (CuxSyOz). The choice of agitation leaching in this mine is based on the mineralogy of the ore body, the topography of the mine site, and current economic conditions.

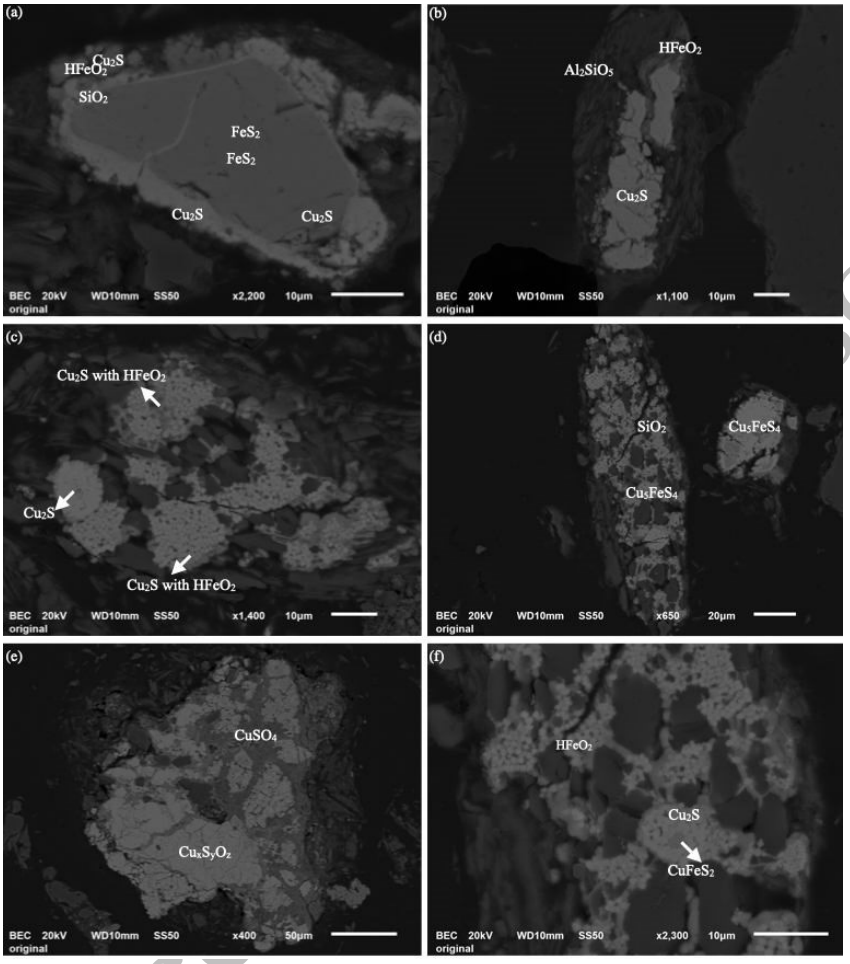

Figure 9. SEM-EDS photomicrographs of copper ore before leaching

4.2 Leaching process experiments and results discussion

Leaching experiments were conducted in a leaching tank where 1.16 kg of the sample was kept in suspension with the lixiviant by mechanically agitating the slurry. The lixiviant consisted of 3L distilled water (with a solid-to-liquid ratio of 0.4), 0.23 kg ferric sulfate ($Fe_3SO_4.xH_2O$; 19.5% Fe^{3+}), and 26 ml sulfuric acid (95%-98%w) from J.T. Baker. The initial concentration of Fe^{3+} and H^+ in the aqueous solution was 15g/L. A 10 ml slurry sample was withdrawn from the tank at 3, 5, 10, 30, 45, 60, 90, and 120 min. The liquid samples were filtered and diluted for assay. All solid samples were filtered, cleaned, dried, and prepared for Cu^{2+} assay.

The effects of leaching temperature on copper recovery were investigated in a laboratory setup. The results in Table 4 demonstrated that temperature variation significantly enhances Cu recovery. At 70 °C, 56.7% of copper was extracted in the first 20 min and eventually exceeded 91% after 120 min, while only 35.4% copper recovery was achieved in 20 min and 51.8% in 120 min at ambient temperature. The new solar collector can easily supply a high leaching temperature, significantly improving the efficiency of copper extraction compared to the process at ambient temperature. Thus, 70°C meets the temperature requirement for the Cu leaching process, which is expected to operate within a temperature range of 50-80°C.

Table 4. Cu recovery in different leaching temperature.

Time(min)	3	5	10	20	30	45	60	90	120
Tempera-ture				Cu extraction (%)					
25 ºC	14.7	16.8	25.2	35.4	44.0	45.8	53.3	51.1	51.8
50 ºC	16.7	19.8	27.2	45.2	51.6	55.5	63.1	71.3	75.4
60 ºC	20.7	25.9	35.8	52.2	60.5	65.7	74.3	79.8	83.7
70 ºC	30.5	35.6	40.6	56.7	66.5	78.5	85.5	85.9	91.5

The leaching residue at 70ºC, were examined by SEM-XRD, as shown in Fig.10. It was found that the $CuSO_4$ and non-stoichiometric copper sulfides were completely leached. Moreover, the copper left in the residues remained as CuS, $Cu_{1.4}S$, FeS_2, as well as some primary copper sulfides. as shown in Fig.10(a) and (b), Cu_2S was not leached or was only partially leached to $Cu_{1.4}S$, as the Cu_2S fully encapsulated in iron oxide and pyrite. The layer of iron oxide and pyrite prevented the lixiviant from diffusing to the surface of the CuS, which suppressed the oxidation of CuS to Cu^{2+}. Bornite (Cu_5FeS_4) was also detected, as shown in Fig.10(f). Cu_5FeS_4 is the oxidation product of chalcopyrite ($CuFeS_2$), therefore, it was difficult for $CuFeS_2$ to react completely with H_2SO_4 and Fe^{3+}, even at 70ºC.

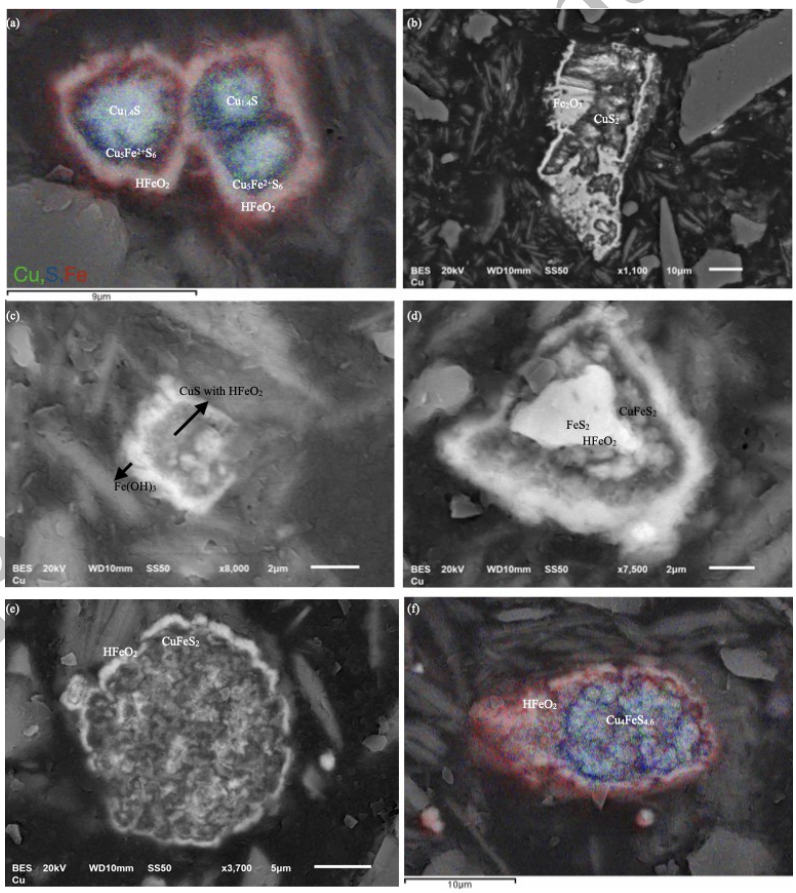

Figure. 10 SEM photomicrographs of leached residue (70ºC)

5. Evaluations of newly designed solar collectors

According to the mineralogy of the ore body, topography of the mine site, and current economic conditions, the agitation leaching is used in Minera Rio Tinto. Agitation leaching is a capital-intensive but very compact technique, in which the ore is suspended in stirring tanks for several hours or days. The 100% of

copper recovery can be approached. As of now, the daily ore feeding is 10 tons, and the leaching time is 3 h. The eventual copper extraction is around 50%, with an annual copper cement production of 26 tons in 2021. The electricity consumption in the agitation leaching process is 1997 MWh based on the power of the water pump and agitator, resulting in 1481 tons of CO_2 emissions.

The solar collector array is intended to be integrated into the existing agitation leaching system. The schematic diagram of the integrated plant is illustrated in Fig.11. The hot water discharged from the solar collectors passes through the spiral heat exchanger to supply the heat needed for leaching. The slurry should remain in the first vat for several hours until its temperature reaches above 70°C. Additionally, fresh sulfuric acid and ferric sulfate are added to oxidize the slurry. Once the slurry temperature reaches 70°C and above, it flows upward into the second vat for further leaching. After 2 h, the slurry flows through the filtration. The pregnant leach solution (PLS) overflows the tank after separation, where the cementation reaction occurs, and the cupric ions convert to copper cements while iron transforms to Fe (II) and Fe (III) ions. The raffinate solution is then pumped back into the first leaching vat to replenish the ferric sulfate.

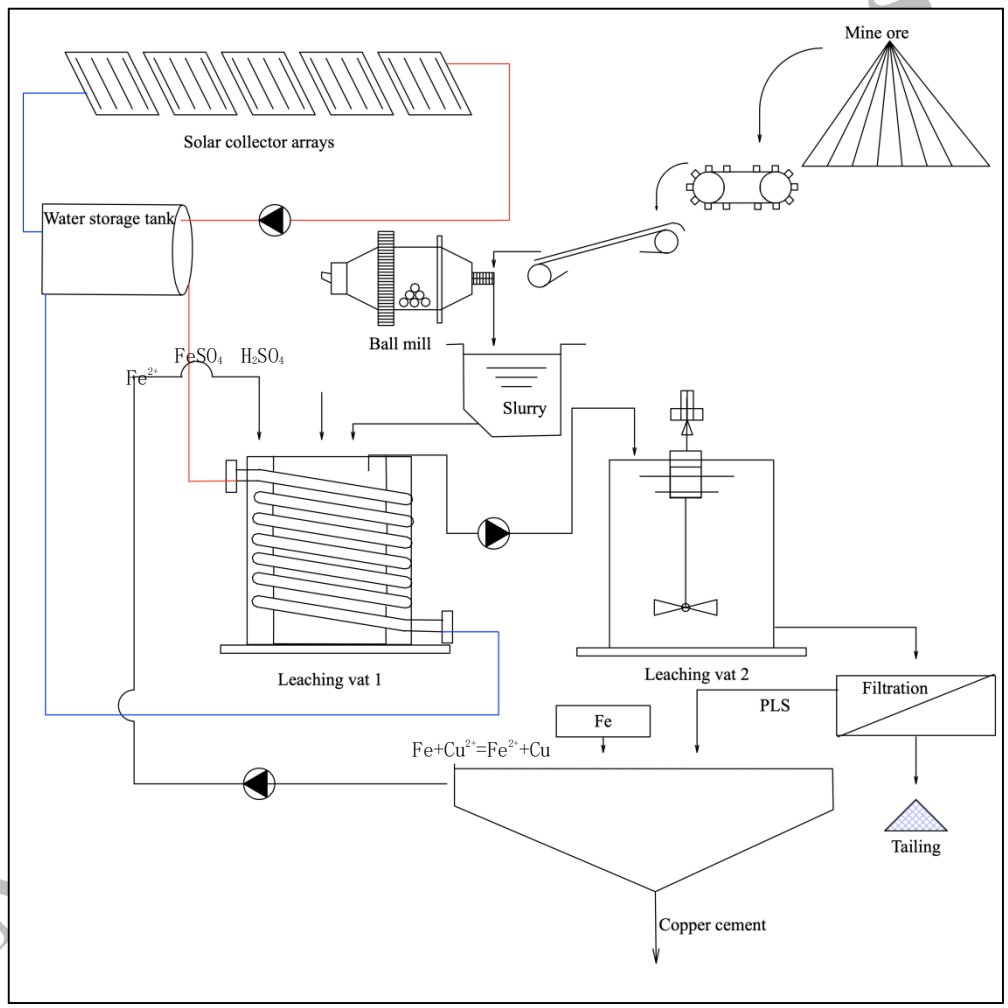

Figure 11. Schematic diagram of the solar agitation leaching operation.

Table 5. Comparison among industrial cases of agitation leaching process.

Rio Tinto, Mexico	Current process	Case 1: New process integrated with solar collectors	Case 2: process integrated with electric heater
Operation			
Cu cement (only leach), t/a	26	73	73
H_2SO_4 consumption, t/t Cu		3.45	
Ore feed to leach			
Average Cu grade, %		Cu 1.45(total), Cu 1.42 (acid-soluble), Cu 0.03(acid-insoluble)	
Ore size to leach, um		80%-174	
Ore fed to leach, t/d	10	15	15
Agitation vats			
No of vats		2	
Impeller power, kW		132	
Water pump power, kW		48	
No of water pump (Leach only)		2	
Electric heater power, kW	-	-	76
Temperature, ^oC	ambient	70	70
Leach residue			
Predominant mineralogy	Major covellite, chalcocite, minor chalcopyrite	Major chalcopyrite, minor covellite	Major covellite, chalcocite, minor chalcopyrite
Cu in residue, %	0.3-0.4	0.15-0.17	0.15-0.17
Leaching efficiency			
Cu recovery (leach only), %	50	91.5	91.5
Residence time of solids in leach, h	3	2	2
Electricity consumption (leach only), MWh/a	1997	1997	2663
CO_2 emission, t/a	1481	1481	1975

Currently, Minera Rio Tinto leaches copper sulfide ore at ambient temperature. If the leaching temperature were increased in the current process, significant improvements would be evident. Table 5 compares the current leaching route with the new solar-leaching and electric heating routes, highlighting key changes.

In comparison to the current route, Case 1 and Case 2 in Table 5 demonstrate that the copper recovery rate after 2 hrs increases from 50% to 91.5% by elevating the leaching temperature from ambient temperature to 70°C. Moreover, the daily ore load increases from 10t to 15t. The eventual cathode copper production rises to 73t/a from 26 t/a, nearly three times greater than the current industrial process. Additionally, the Cu residue after each cycle of leaching in Case 1 and 2 reduces by 50%. In Case 2, it is observed that electric consumption increases by 16.7% compared to the new solar energy process in Case 1, and CO_2 emissions also increase by 17% due to the electric heater. Thus, the application of new solar energy in the Cu leaching process is proven to be cost-effective, efficient, and environmentally friendly.

The economic and environmental advantages offered by the solar thermal system make the new solar collector particularly attractive provided its capital cost remains reasonable. In this study, the reflector geometry was designed as a half-spherical curve and a strength line, constituting a solar thermal system comprising 25 solar collectors and a 1000L water tank. The manufacturing costs are itemized and presented in Table 6 for transparency. A comparison with three other designs from the literature [21], considering optical efficiency and manufacturing cost, reveals that their optical efficiency ranged from 0.5 to 0.8, with unit costs between \$125 and \$490. In contrast, our newly designed collectors boast an optical efficiency of 0.73, as discussed in the previous section. The CPC collector arrays comes at a cost of \$2990 USD for 25 solar collectors, translating to a remarkably low unit cost of \$119 USD per collector. The total cost of the system is \$3,127 USD, which includes five solar collector arrays (totaling \$2,990 USD) and a 1,000L water tank priced at \$137, results in a cost of \$125 USD /m^2.

The payback period is the amount of time it takes for the savings to cover the initial investment. It can be calculated as:

Payback Period (P) = Initial Investment (C_0) ÷ Annual Savings (C_s)

Based on the energy cost of natural gas in Mexico, the energy produced by the solar thermal system annually (based on solar radiation, collector efficiency, etc.), the payback period of the collector was estimated to be approximately 5.4 years. The detailed calculation process is provided in Appendix 2. This cost-effectiveness, coupled with superior optical efficiency, positions the new solar collector as a promising solution for sustainable energy applications.

Table 6 Manufacture cost of the CPC collector-array

Material	Use	Cost per unit \$USD	Units	Cost \$USD
A CPC collector-array (including 5 CPC-type collector)				
Aluminum sheet 3003	CPC structure	15 /m^2	8.16m^2	122
Polyurethane	Concentrator	6.75/L	20L	135
Copper tube	Heat receiver	40 c/u	5	200
Polycarbonate plane	Enclosure, supporter	16.35/m	3.5m	57
Tee tube plus 40mm	connection	1.55c/u	5	7.75
Connection of tube plus	connection	various	various	20
Tube plus 20mm	connection	0.75/m	6.6m	4.95
connector		various	various	10
Stainless Steel T Bolt Clamp	connection	0.65c/u	64	41.6
Total				598
A 1000L water tank				
Polyethylene water tank		80c/u	1	80
Aluminum sheet 3003	Enclosure	16.35/m	3.51	57
A thermal system				
CPC collector array		**598 c/u**	**5**	**2990**

A 1000L water tank	137 c/u	1	137
Total			**3127**
Payback period			5.4years

6. Conclusions and future work

In this study, we successfully developed an efficient and practical solar concentrator designed for the copper leaching process in copper mines. The newly configured solar concentrator, employing a spherical curve connected with a straight line, was meticulously constructed, evaluated, and subjected to comprehensive performance analysis. The concentrators demonstrated the capability to collect solar irradiation throughout the year without relying on tracking systems. The following conclusions are drawn:

1. The optical efficiency of our new solar collector reaches 0.73, accompanied by a maximum thermal efficiency of 68%. This new Solar Thermal Collector (STC) proves to be efficient, cost-effective, and easily manufacturable, contributing to the enhancement of copper recovery in leaching processes.
2. The newly developed solar collector can generate 1000L of hot water using a 25 m^2 of solar collector area. Heating the water to 80ºC and maintaining it at 70ºC for the subsequent 24 h.

The investigation showcased a novel integrated solar collector with an agitation leaching system, demonstrating significant economic benefits in a case study of leaching production. The unit cost of this new solar collector is a mere $119 USD, the entire system is $125 USD/$m^2$, leading to a substantial reduction in capital costs.

Integration of the new concentrator with the copper leaching process in a Mexican mining industry would result in a substantial improvement in copper recovery. The recovery rate at 70°C would increase to 91.5% from 50%, subsequently raising the daily ore load from 10t to 15t. The eventual copper cement production would surge from 26 t/a to 73t/a, nearly three times greater than current industrial processes. Importantly, CO2 emissions would remain unchanged. The feasibility of the new concentrators at an industrial scale is conducive to promoting further innovation in cleaner copper production technology.

This study would encourage further studies in higher efficient solar concentrators with low costs. We considered only the manufacturing cost in this study and further economic analysis such as operating cost, end-of-life cost, and maintenance cost could be investigated. An improvement of optical design to increase the optical efficiency such as minimizing gap losses could be explored. Scaling up the laboratory solar collector to a pilot plant is a crucial future application to advance efficient, effective, and carbon neutral copper leaching. Additionally, we plan to study on the cementation process by utilizing a new solar concentrator to transform solar radiation into heat.

Acknowledgments: This work was funded by the project CEMIE-SOL P066 and the National Council for Science and Technology, Mexico (CONACyT). Mineral ores and support from Minera Río Tinto, Chihuahua, México to conduct this work is fully acknowledged.

Appendix 1

The CO_2 emissions can be calculated using equation below:

The carbon dioxide emissions：

CO_2（kg）=kWh·0.742

Where, the conversion factor was 0.742 tCO_2/MWh for coal-fired power plants at Mexico [22]. Once obtain the amount of electricity consumed, typically measured in (kWh), multiply the conversion factor to get the total CO_2 emissions.

In the case of not using electric heating, the leaching process employs two water pumps with a power of 48 kW each and one impeller agitator with a power of 132 kW. Assuming the leaching process operates 24 h a day and 365 days a year, the annual power consumption is calculated as 1997 MWh. The corresponding

carbon dioxide emissions are calculated based on an emission conversion factor related to electricity consumption.

Appendix 2

Initial cost of the solar thermal system = $3127 USD
Cost of energy = $0.027 USD/kWh (2024 natural gas prices of Mexico)
Solar Radiation Availability for San Luis Potosí = 5.6 kWh/m^2/day
Average thermal efficiency of the CPC = 0.42
The effective thermal = 0.42 * 5.6 kWh/m^2/day *25 m^2= 58.8 kWh/ day
Daily Energy saving = (58.8 kWh/ /day) * ($0.027 USD/kWh) = $1.59 USD/ day
Payback period = Initial cost of the solar system / Daily Energy saving = $3127 USD/$1.59 USD/day= 5.4 years

Authors´ contributions

Ke Yang: Original draft. Investigation. Formal analysis. Resources. Data Curation. Visualization
Yuri Nahmad Molinari: Validation.Resources. Writing - Review & Editing. Funding acquisition
Luis Fernando Camacho Conzález: Software. Visualization
Fátima MI de los Santos García: Validation.
Alejandro Lopéz Valdivieso: Conceptualization. Methodology. Validation. Writing - Review and Editing. Supervision.

Data availability

Data are available on request to the authors.

Conflict of interest

All authors disclosed no relevant relationships.

Reference

1. Change, U.N.C. *Paris Agreement*. 2021 [cited 2021 15 July]; Available from: https://treaties.un.org/Pages/ViewDetails.aspx?src=TREATY&mtdsg_no=XXVII-7-d&chapter=27&clang=_en.

2. Wang, F., et al., *Low-loading Pt nanoparticles combined with the atomically dispersed FeN(4) sites supported by Fe(SA)-N-C for improved activity and stability towards oxygen reduction reaction/hydrogen evolution reaction in acid and alkaline media.* J Colloid Interface Sci, 2023. **635**: p. 514-523.doi.org/10.1016/j.jcis.2022.12.160

3. Li, Q., et al., *Sediment Instability Caused by Gas Production from Hydrate-bearing Sediment in Northern South China Sea by Horizontal Wellbore: Evolution and Mechanism.* Natural Resources Research, 2023. **32**(4): p. 1595-1620.doi.org/10.1007/s11053-023-10202-7

4. Li, Q., et al., *Effect of reservoir characteristics and chemicals on filtration property of water-based drilling fluid in unconventional reservoir and mechanism disclosure.* Environ Sci Pollut Res Int, 2023. **30**(19): p. 55034-55043.doi.org/10.1007/s11356-023-26279-9

5. Agency, T.I.E. *Industry*. 2023; Available from: https://www.iea.org/energy-system/industry.

6. Jiang C, et al., *A Review of the Compound Parabolic Concentrator (CPC) with a Tubular Absorber.* Energies, 2020. **13(3)**: p. 695.doi.org/https://doi.org/10.3390/en13030695

7. Azad Gilani, H. and S. Hoseinzadeh, *Techno-economic study of compound parabolic collector in solar water heating system in the northern hemisphere.* Applied Thermal Engineering, 2021. **190**: p. 116756.doi.org/https://doi.org/10.1016/j.applthermaleng.2021.116756

8. Ahmadi, A., et al., *Recent progress in thermal and optical enhancement of low temperature solar collector.* Energy Systems, 2023. **14**(1): p. 1-40.doi.org/10.1007/s12667-021-00473-5

9. Martín-Sómer, M., et al., *High-performance low-cost solar collectors for water treatment fabricated with recycled materials, open-source hardware and 3d-printing technologies.* Science of The Total Environment, 2021. **784**: p. 147119.doi.org/https://doi.org/10.1016/j.scitotenv.2021.147119

10. Jena, S.S., et al., *Sustainable Use of Copper Resources: Beneficiation of Low-Grade Copper Ores.* Minerals, 2022. **12**(5): p. 545

11. Watling, H.R., et al., *Leaching of a low-grade, copper–nickel sulfide ore. 1. Key parameters impacting on Cu recovery during column bioleaching.* Hydrometallurgy, 2009. **97**(3): p. 204-212.doi.org/https://doi.org/10.1016/j.hydromet.2009.03.006

12. Ji, G., et al., *A review on the research of hydrometallurgical leaching of low-grade complex chalcopyrite.* Journal of Sustainable Metallurgy, 2022. **8**(3): p. 964-977.doi.org/https://doi.org/10.1007/s40831-022-00561-5

13. Javanshir, S., H. Imantalab, and M. Fathi, *Accelerating copper leaching from a complex ore containing atacamite: optimisation and kinetic studies.* Canadian Metallurgical Quarterly: p. 1-12.doi.org/10.1080/00084433.2023.2171675

14. Pérez, K., et al., *Leaching of Pure Chalcocite in a Chloride Media Using Waste Water at High Temperature.* Metals, 2020. **10**(3): p. 384.doi.org/https://doi.org/10.3390/met10030384

15. *Energy efficiency • Energy intensity in copper and gold mining*. 2017; Available from: https://www.at-minerals.com/en/artikel/at_-3001684.html.

16. Bellos, E., et al., *Design, simulation and optimization of a compound parabolic collector.* Sustainable Energy Technologies and Assessments, 2016. **16**: p. 53-63.doi.org/https://doi.org/10.1016/j.seta.2016.04.005

17. Jiang PT, et al., *The fundamental performance of FAST with 19-beam receiver at L band.* Research in Astronomy and Astrophysics, 2020. **20**(5): p. 064.doi.org/10.1088/1674-4527/20/5/64

18. O'Gallagher, J., *Nonimaging optics in solar energy*. Vol. 2. 2008: Morgan & Claypool Publishers

19. John A. Duffie and W.A. Beckman, *Available Solar Radiation*, in *Solar Engineering of Thermal Processes*. 2013. p. 43-137.

20. Reda, I.A., A. , *Solar Position Algorithm for Solar Radiation Applications.* . NREL Report No. TP-560-34302,, 2008: p. 55 pp

21. Jannesari, H. and B. Babaei, *Optimization of solar assisted heating system for electro-winning process in the copper complex.* Energy, 2018. **158**: p. 957-966.doi.org/10.1016/j.energy.2018.06.119

22. Mechanism, J.C. *Installation of Solar PV System*. 2017; Available from: https://www.jcm.go.jp/mx-jp/methodologies/62.

Figures

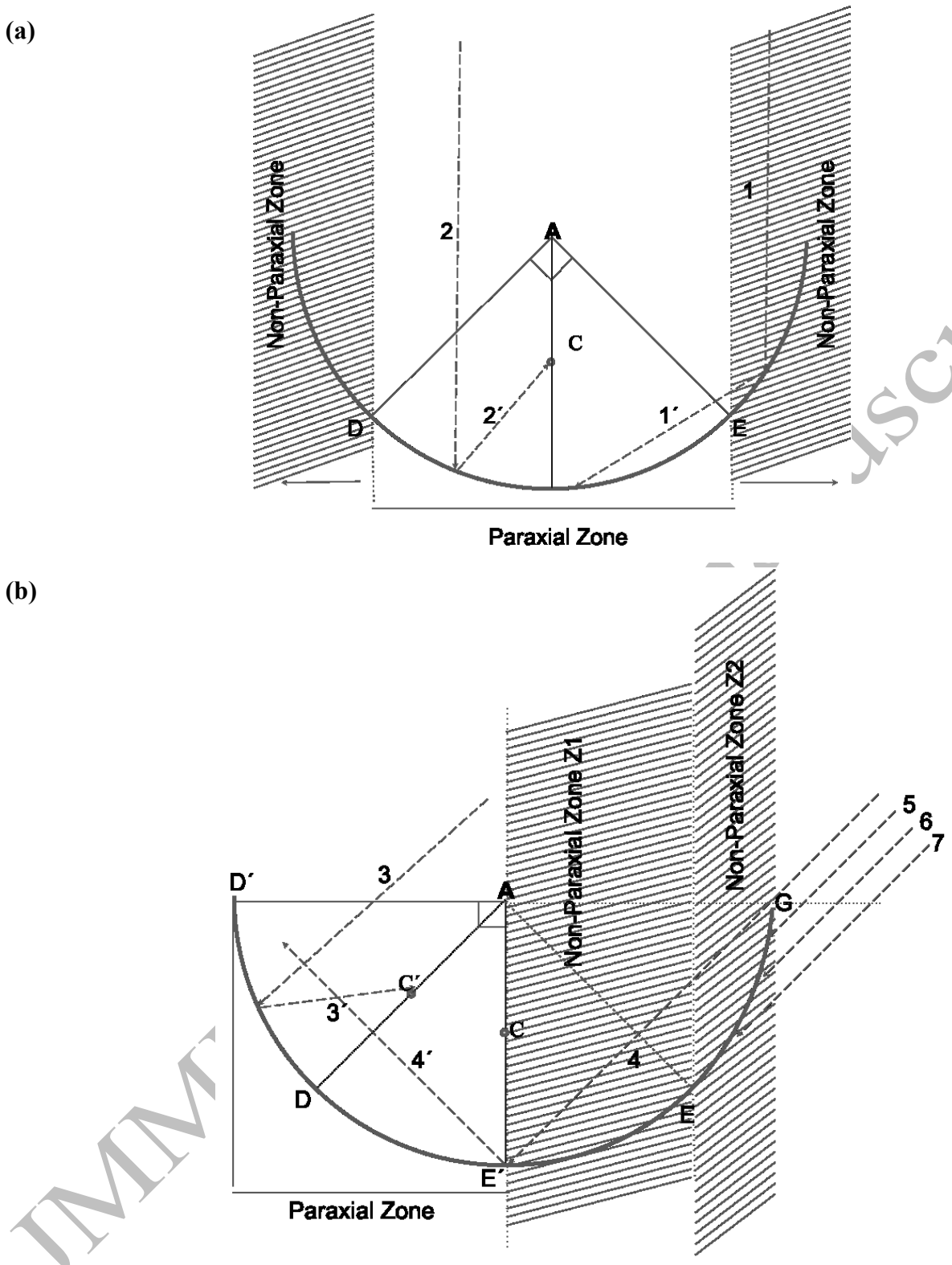

Fig.1 Geometry of the CPC-type concentrator: (a) in summer solstice and (b) in winter solstice

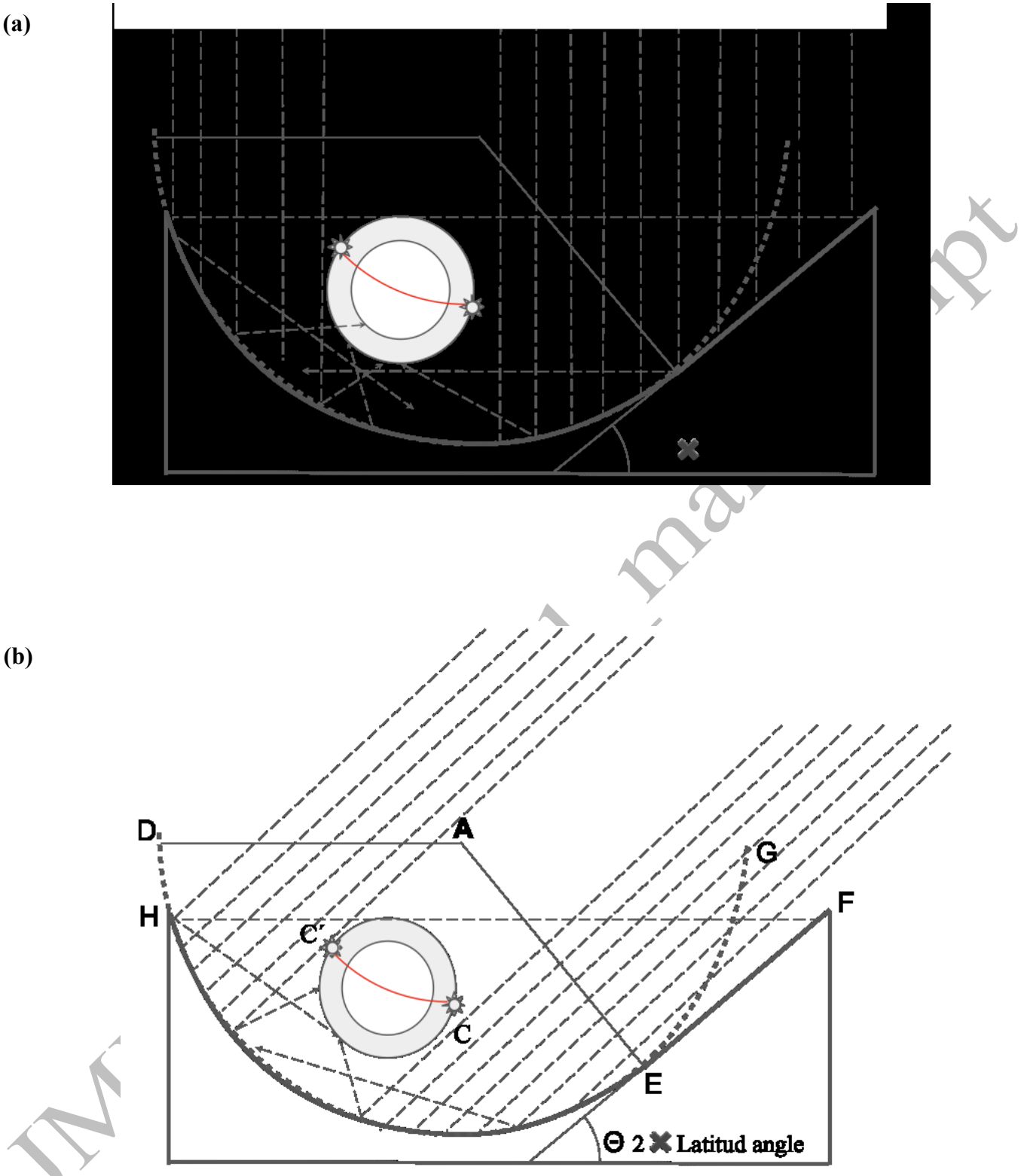

Fig.2 Illustration of ray tracing for the CPC-type concentrator: (a) in summer solstice and (b) in winter solstice

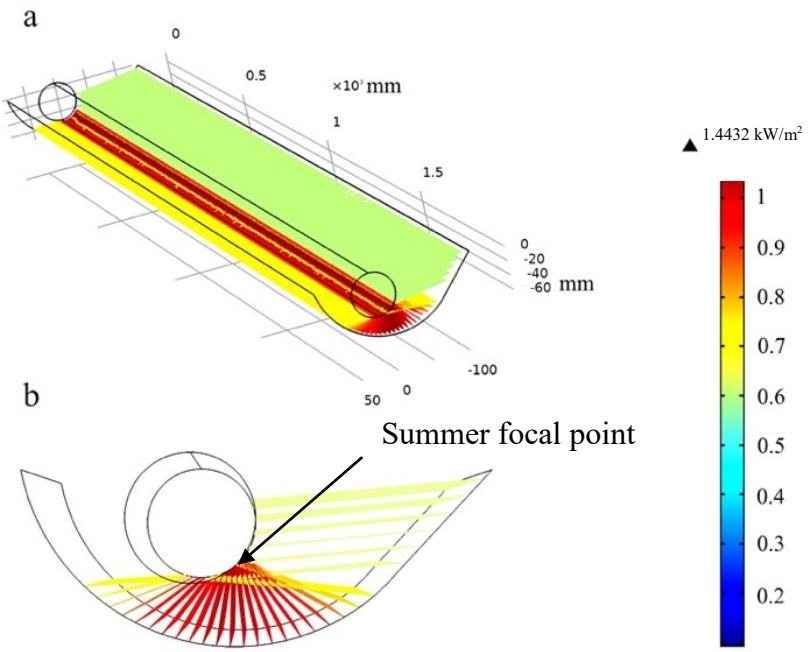

Fig.3 (a) Solar flux distribution on the absorber surface and

(b) cross-section at summer solstice

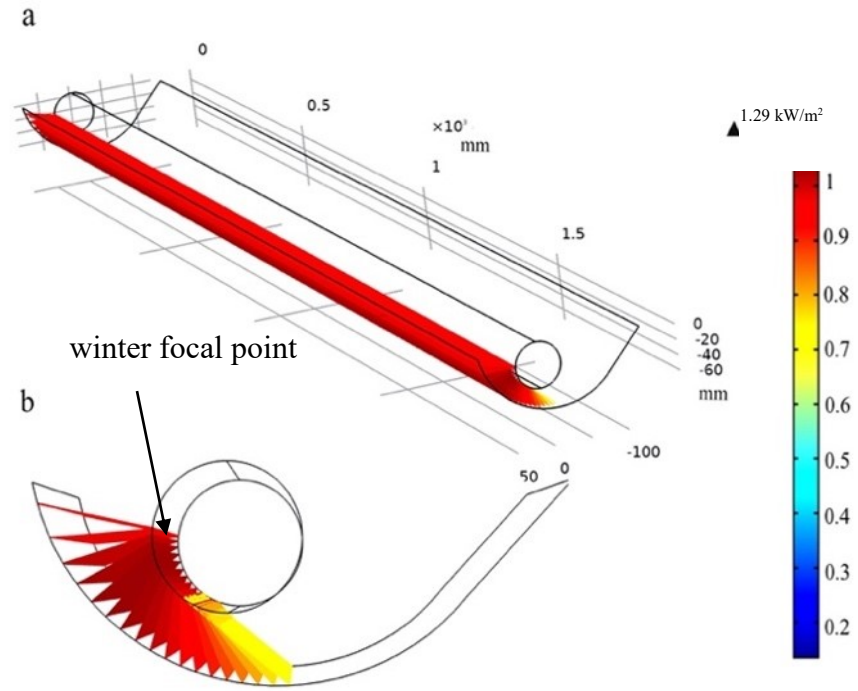

Fig.4 (a) Solar flux distribution on the absorber surface and

(b) cross-section at winter solstice

Fig.5 The new concentrator

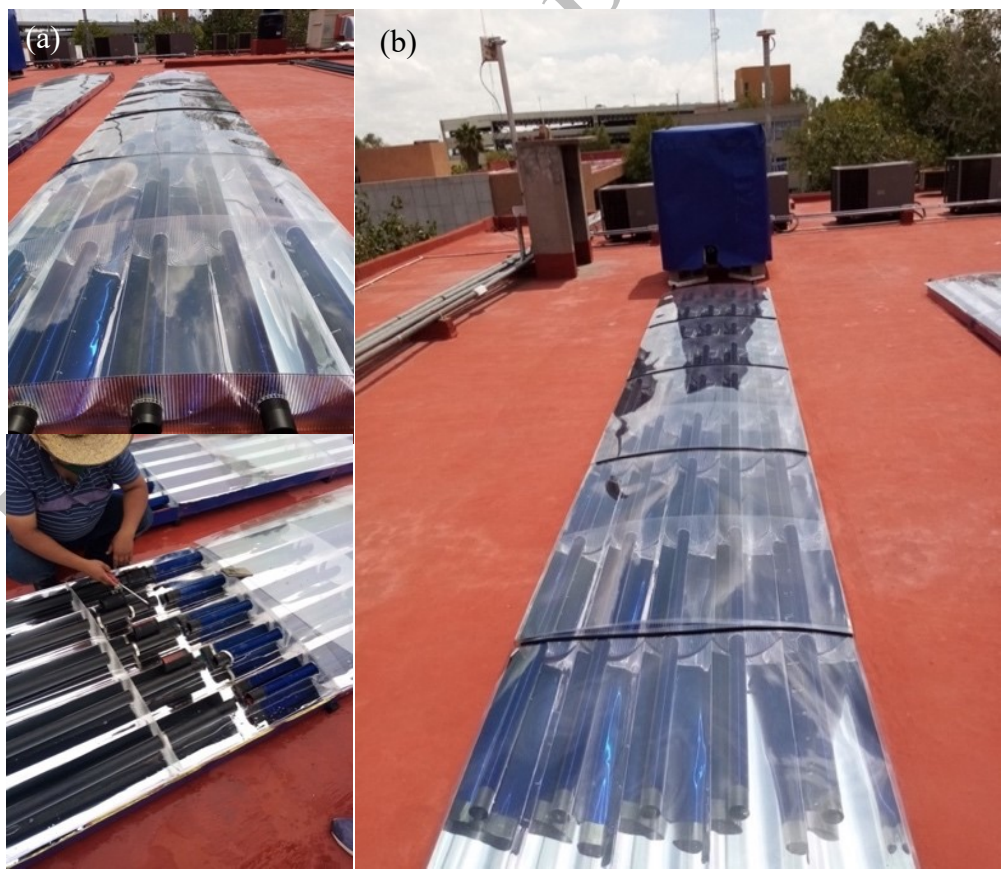

Fig.6 (a) New solar collector (a) Overall and internal structure of collector; (b) Water tank and collector.

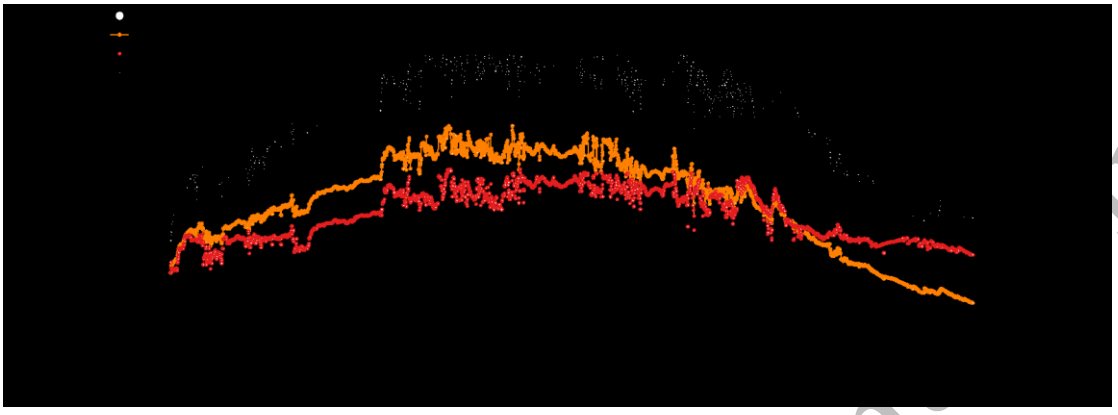

Figure 7. Solar irradiation within a daily test in San Luis Potosi, Mexico on March 20, 2023.

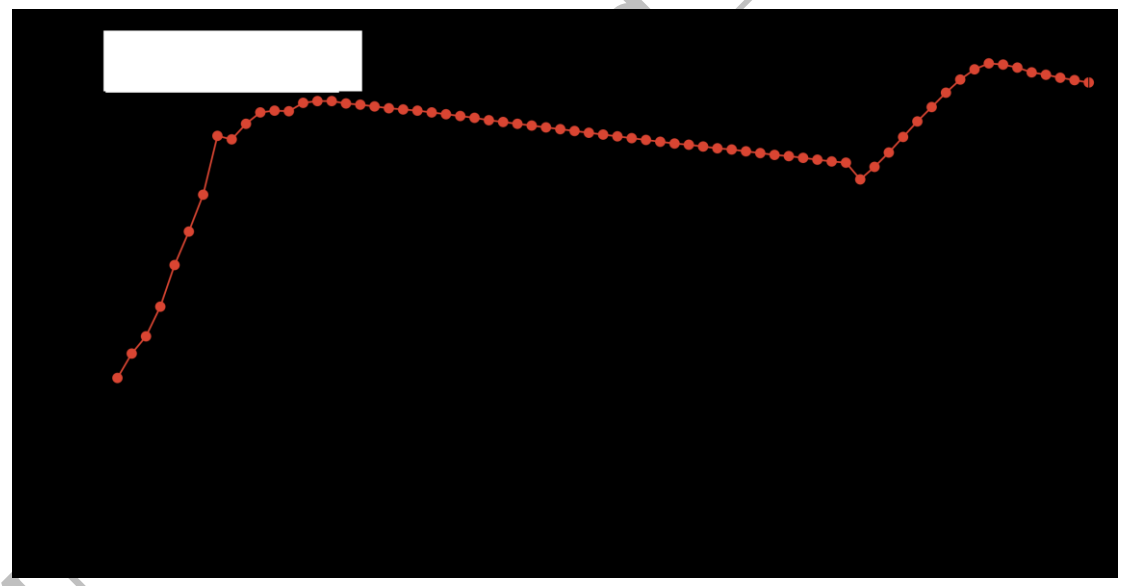

Figure 8. Water temperature change as a function of solar time in San Luis Potosi, Mexico.

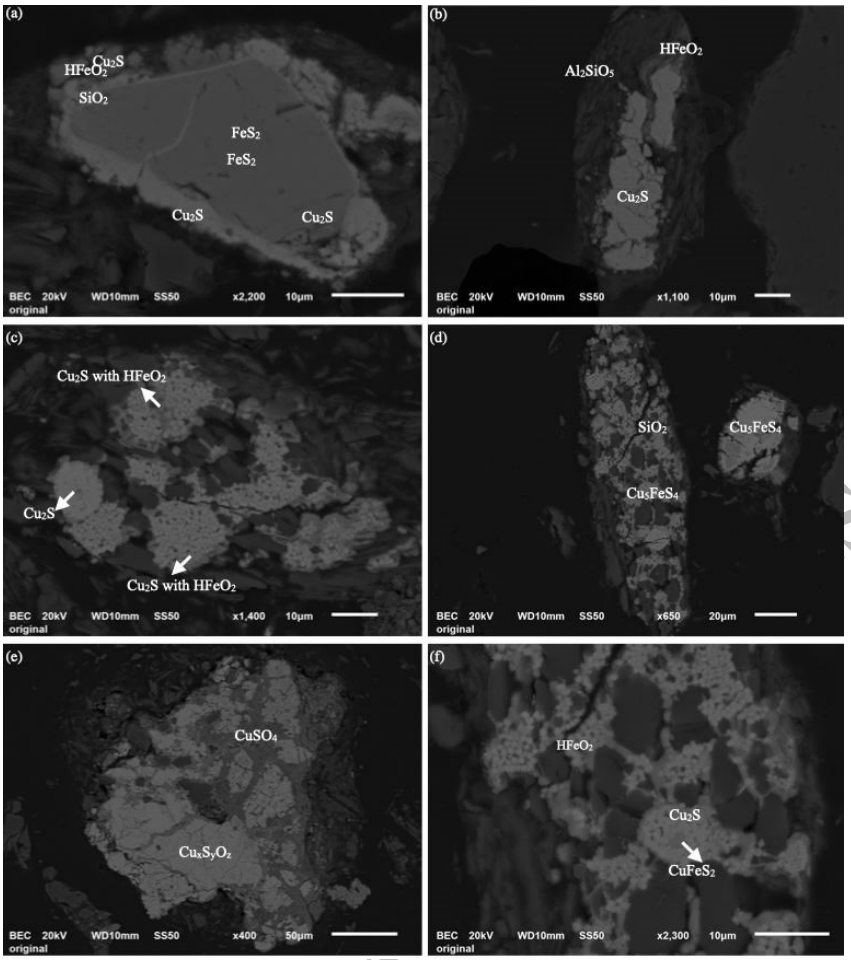

Figure 9. SEM-EDS photomicrographs of copper ore before leaching

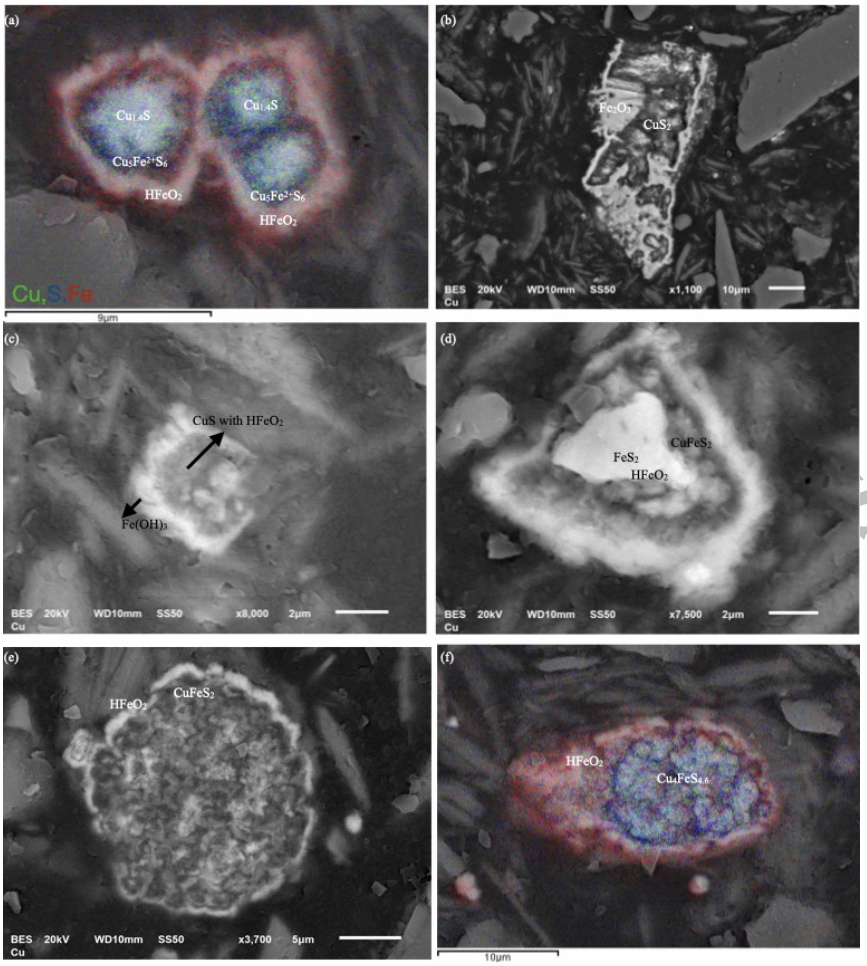

Figure. 10 SEM photomicrographs of leached residue (70ºC)

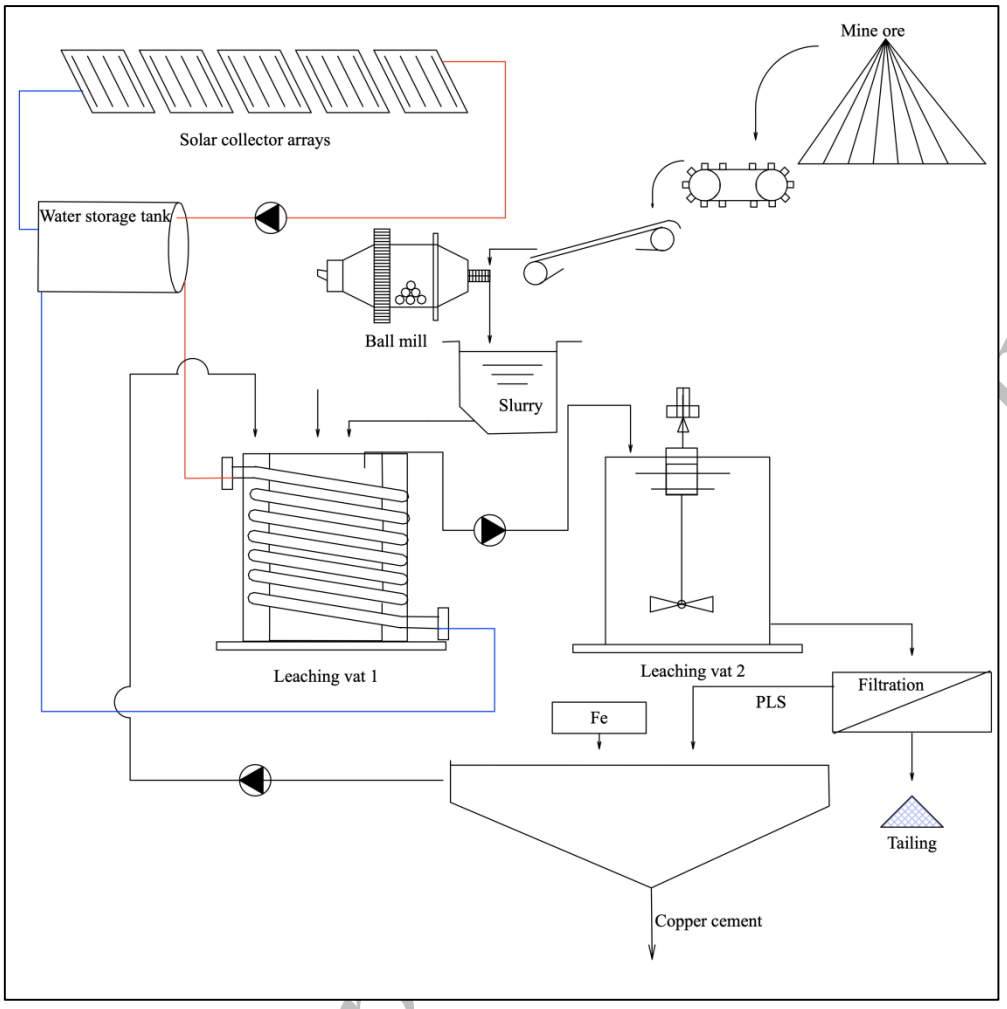

Fig.11 Schematic diagram of the solar-agitation leaching operation

Tables

Table 1. Geometry of the new concentrator

Parameters	The nonsymmetric CPC
Width of the collector	0.22m
Length of the collector	1.8m
Height of the collector	0.1m
Curvature radius of the half-spherical curve	0.10m

Table 2 Performance Parameters for concentrator

Parameter	symbol	Value
Transmittance of outer envelope of the heat receiver (polycarbonate)	$\tau 1$	0.9
The reflectivity of the concentrator surface (Alumina)	$\tau 2$	0.95
Average number of reflections	(n)	0.8
Absorptance of coating surface	α	0.95
Gap loss	L	0.076 (Eq.3)
Correction for loss of diffuse	Γ	0.97
Optical efficiency	$\eta_{optical}$	0.73 (Eq.1)

Table 3 Chemical composition of the copper sulfide ore sample

	Mineral					Total
	Copper soluble in water	Copper soluble in acetic acid	Copper oxide	Secondary copper sulfide	Primary Copper sulfide	
Ore assay %	0.026	0.284	0.330	0.780	0.030	1.45
Distribution %	1.79	19.59	22.76	53.79	2.07	100

Table 4. Cu recovery in different leaching temperature.

Time(min)	3	5	10	20	30	45	60	90	120
Temperature	Cu extraction (%)								
25 ºC	14.7	16.8	25.2	35.4	44.0	45.8	53.3	51.1	51.8
50 ºC	16.7	19.8	27.2	45.2	51.6	55.5	63.1	71.3	75.4
60 ºC	20.7	25.9	35.8	52.2	60.5	65.7	74.3	79.8	83.7
70 ºC	30.5	35.6	40.6	56.7	66.5	78.5	85.5	85.9	91.5

Table 5. Comparison among industrial cases of agitation leaching process.

Rio Tinto, Mexico	Current process	Case 1: New process integrated with solar collectors	Case 2: process integrated with electric heater
Operation			
Cu cement (only leach), t/a	26	73	73
H_2SO_4 consumption, t/t Cu		3.45	
Ore feed to leach			
Average Cu grade, %		Cu 1.45(total), Cu 1.42 (acid-soluble), Cu 0.03(acid-insoluble)	
Ore size to leach, um		80%-174	
Ore fed to leach, t/d	10	15	15
Agitation vats			
No of vats		2	
Impeller power, kW		132	
Water pump power, kW		48	
No of water pump (Leach only)		2	
Electric heater power, kW	-	-	76
Temperature, ºC	ambient	70	70
Leach residue			
Predominant mineralogy	Major covellite, chalcocite, minor chalcopyrite	Major chalcopyrite, minor covellite	Major covellite, chalcocite, minor chalcopyrite
Cu in residue, %	0.3-0.4	0.15-0.17	0.15-0.17
Leaching efficiency			
Cu recovery (leach only), %	50	91.5	91.5
Residence time of solids in leach, h	3	2	2
Electricity consumption (leach only), MWh/a	1997	1997	2663
CO_2 emission, t/a	1481	1481	1975

Table 6 Manufacture cost of the CPC collector-array

Material	Use	Cost per unit US$	Units	Cost US$
A CPC collector-array (including 5 CPC-type collector)				
Aluminum sheet 3003	CPC structure	15 /m^2	8.16m^2	122
Polyurethane	Concentrator	6.75/L	20L	135
Copper tube	Heat receiver	40 c/u	5	200
Polycarbonate plane	Enclosure, supporter	16.35/m	3.5m	57
Tee tube plus 40mm	connection	1.55c/u	5	7.75
Connection of tube plus	connection	various	various	20
Tube plus 20mm	connection	0.75/m	6.6m	4.95
connector		various	various	10
Stainless Steel T Bolt Clamp	connection	0.65c/u	64	41.6
Total				598
A 1000L water tank				
Polyethylene water tank		80c/u	1	80
Aluminum sheet 3003	Enclosure	16.35/m	3.51	57
A thermal system				
CPC collector array		598 c/u	5	2990
A 1000L water tank		137 c/u	1	137
Total				3127